HHS Public Access

Author manuscript

Dev Neurobiol. Author manuscript; available in PMC 2016 June 01.

Published in final edited form as:

Dev Neurobiol. 2015 June ; 75(6): 621–640. doi:10.1002/dneu.22288.

Spatial pattern of spontaneous retinal waves instructs retinotopic map refinement more than activity frequency

Hong-Ping Xu[1,4], **Timothy J. Burbridge**[1,4], **Ming-Gang Chen**[2], **Xinxin Ge**[1], **Yueyi Zhang**[1], **Z. Jimmy Zhou**[2], and **Michael C. Crair**[1,2,3,*]

[1]Department of Neurobiology

[2]Department of Ophthalmology and Visual Science

[3]Kavli Institute of Neuroscience

Abstract

Spontaneous activity during early development is necessary for the formation of precise neural connections, but it remains uncertain whether activity plays an instructive or permissive role in brain wiring. In the visual system, retinal ganglion cell (RGC) projections to the brain form two prominent sensory maps, one reflecting eye of origin and the other retinotopic location. Recent studies provide compelling evidence supporting an instructive role for spontaneous retinal activity in the development of eye-specific projections, but evidence for a similarly instructive role in the development of retinotopy is more equivocal. Here, we report on experiments in which we knocked down the expression of β2-containing nicotinic acetylcholine receptors (β2-nAChRs) specifically in the retina through a Cre-loxP recombination strategy. Overall levels of spontaneous retinal activity in retina-specific β2-nAChR mutant mice (Rx-β2cKO), examined *in vitro* and *in vivo*, were reduced to a degree comparable to that observed in whole animal β2-nAChR mouse mutants (β2KO). However, many residual spontaneous waves in Rx-β2cKO mice displayed local propagating features with strong correlations between nearby but not distant RGCs typical of waves observed in WT, but not β2KO mice. We further observed that eye-specific segregation was disrupted in Rx-β2cKO mice, but retinotopy was spared in a competition-dependent manner. These results suggest that propagating patterns of spontaneous retinal waves are essential for normal development of the retinotopic map, even while overall activity levels are significantly reduced, and support an instructive role for spontaneous retinal activity in both eye-specific segregation and retinotopic refinement.

Introduction

The development of complex features of the vertebrate nervous system is governed by a combination of genetic factors and neuronal activity (Huberman et al., 2008; Sanes and Zipursky, 2010; Kirkby et al., 2013). A well-known example is the development of connections from the retina to the brain. Retinal ganglion cell (RGC) projections are first guided by molecular cues to form crude visual maps, which then undergo a substantial

*Correspondence: michael.crair@yale.edu.

[4]Co-first authors

structural remodeling to achieve their adult pattern of functional connectivity (McLaughlin and O'Leary, 2005; Feldheim and O'Leary 2010; Huberman et al., 2008; Ackman and Crair, 2014). For instance, axons from the two eyes initially overlap and then gradually segregate to innervate distinct regions of shared brain targets (Godement et al., 1984; Penn et al., 1998; Stellwagen and Shatz 2002). This eye-specific segregation is accompanied by the development of retinotopy, in which RGC axons first project broadly, but then restrict their arbors to smaller target areas where adjacent axons maintain the same relative spatial relationship of their parent cell bodies in the retina (McLaughlin et al., 2003; Grubb et al., 2003; Mrsic-Flogel et al., 2005; Chandrasekaran et al., 2005).

The refinement of RGC axon projections for eye-specific segregation and retinotopy are both partially regulated by neuronal activity that originates in the retina. During early development, before the onset of visual experience, immature retinal circuits periodically discharge correlated activity that propagates in a wave-like manner across large swathes of the retina, and so are referred to as retinal waves (Meister et al., 1991; Feller et al., 1996; Ackman et al., 2012). Manipulations designed to chronically eliminate retinal waves during periods of visual circuit refinement cause disrupted eye-specific segregation and retinotopy (Huberman et al., 2008; Ackman and Crair, 2014; Burbridge et al., 2014). Despite the necessity of patterned retinal activity for the normal maturation of retinotopy and eye-specific segregation, the specific mechanism whereby retinal waves modulate circuit development remains uncertain (Crair, 1999; Cline, 2003; Chalupa, 2009 and Feller, 2009). One essential remaining question is whether spontaneous activity acts in a "permissive" way to simply allow cell survival and neurite outgrowth, or in an "instructive" way to directly promote and guide circuit formation (Crair, 1999; Xu et al., 2011). Answering this question is challenging, as it requires manipulations that specifically alter the pattern of spontaneous activity without affecting overall levels of neuronal activity and the converse.

Retinal waves are divided into three developmental stages that are mediated by three transient retinal circuits (Wong, 1999; Firth et al., 2005; Huberman et al., 2008). Cholinergic waves, the second stage of spontaneous activity, occur during the first postnatal week in mice (Feller et al., 2006; Zheng et al., 2006) and are critical for normal visual circuit development. Genetic deletion of the β2 subunit of nicotinic acetylcholine receptors (nAChRs) or pharmacological blockade of functional nAChRs eliminates cholinergic retinal waves and disrupts the formation of retinotopic maps and eye-specific segregation throughout the visual pathway (McLaughlin et al., 2003; Grubb et al., 2003; Mrsic-Flogel et al., 2005; Chandrasekaran et al., 2005; Torborg CL and Feller, 2006; Xu et al., 2011; Burbridge et al., 2014). However, these manipulations change both the spatiotemporal pattern and the overall activity level of spontaneous retinal activity, making it difficult to distinguish between a passive and an active role for neuronal activity in visual map development.

We recently provided evidence in support of an instructive role for spontaneous wave activity in the development of eye-specific segregation (Xu et al., 2011; Burbridge et al., 2014). Using a tetracycline controlled transcriptional system, we generated β2(TG) mice in which β2 subunits are restored to retinal neurons in a β2 germline knockout mouse. Although RGC spiking rates in β2(TG) mice are restored to nearly normal levels, wave

propagation is truncated and eye-specific projections remain poorly segregated. These results suggest that merely the presence of normal levels of spontaneous activity is not sufficient for normal segregation, but that specific spatiotemporal patterns and large-scale correlations of spontaneous activity are necessary for the development of eye-specific projections. Curiously, development of the retinotopic map is not affected by truncated waves in β2(TG) mice. This suggests that locally correlated spontaneous activity is sufficient for retinotopic refinement of RGC axon arbors, but not eye-specific segregation. However, these results failed to distinguish between the necessity of local activity correlations (or the spatiotemporal pattern) of spontaneous activity and overall spike rates in the development of normal retinotopy.

Mice with a germ line deletion of the β2 subunit of the nAChR (*Chrnb2* KO or β2KO mice) have greatly disrupted eye-specific segregation and retinotopy, and spontaneous activity that is dramatically altered as observed both *in vitro* (Bansal et al. 2000, but see Sun et al., 2008; Stafford et al., 2009) and *in vivo* (Burbridge et al., 2014). Retinal neurons in β2 knockout mice (β2KO) maintain a low level of non-cholinergic spontaneous activity during the first postnatal week that has dramatically altered spatiotemporal properties. β2KO activity patterns are more globally correlated, with propagation speeds that are much faster than cholinergic waves, making the activity seem more “flash”-like, than wave-like. Moreover, chronic pharmacological rescue of overall activity levels in β2KO mice fails to rescue topographic map disruptions, but partially rescues eye-specific segregation, implying both that overall activity levels are more important for eye-specific segregation and that the spatiotemporal properties of retinal waves might be more instructive for retinotopy (Burbridge et al., 2014). Therefore, it remains unclear whether activity levels and/or wave dynamics are more important for determining visual circuit refinement, particularly with respect to retinotopy.

In this study, we aimed to clarify these possibilities by reducing neuronal activity levels during cholinergic waves, while maintaining appropriate spatial correlations between neighboring RGCs. To achieve this, we used conditional mouse mutants to manipulate spontaneous activity such that RGCs fired at low levels, but the correlation properties of neighboring RGCs were largely maintained. We found that retinotopic maps developed normally even though overall activity levels were reduced to levels comparable to those observed in β2 (whole animal) knockout mice, suggesting that locally correlated and normally propagating spontaneous retinal activity, even at low overall levels, is necessary and sufficient for activity-dependent retinotopic refinement.

Materials and Methods

Animals

All experimental procedures were in accordance with NIH guidelines and approved by Institutional Animal Care and Use Committees. Animals were treated in compliance with the U.S. Department of Health and Human Services and Yale University School of Medicine. β2-floxed mice have been described in detail previously (Burbridge et al., 2014). These mice possess *loxP* sites flanking approximately 2.2 kb surrounding exon 5 of *Chrnb2*, the largest coding exon (970bp), creating functional nulls when excised by Cre recombinase

(Burbridge et al., 2014). Mice lacking functional β2 subunits in the retina (Rx-β2cKO) were generated by crossing $\beta2^{flox/flox}$ mice with Rx-Cre mice, which express Cre recombinase throughout the retina beginning early (E9) in gestation (Swindell et al., 2006; Dhande et al., 2012). To generate Rx-β2cKO mice, Rx-Cre mice were crossed to $\beta2^{-/-}$ mice (in all *in vitro* anatomy and physiology experiments $\beta2^{-/-}$ mice from Burbridge et al., 2014, but for *in vivo* imaging experiments background was $\beta2^{-/-}$ mice from Xu et al., 1999) to create Rx-Cre^{+}; $\beta2^{+/-}$ mice, which were then crossed to $\beta2^{flox/flox}$ mice to obtain Rx-β2cKO mice (Rx-Cre^{+}; $\beta2^{flox/-}$), littermate WT (Rx-Cre^{-}; $\beta2^{flox/+}$) and Heterozygous (Rx-Cre^{+}; $\beta2^{flox/+}$ and Rx-Cre^{-}; $\beta2^{flox/-}$) controls. tdTomato reporter mice, which have a loxP-flanked STOP cassette that prevents transcription of the downstream red fluorescent protein variant (tdTomato) except in the presence of Cre recombinase, were obtained from The Jackson Laboratory (Stock #007909).

Immunohistology

Cre expression in the retina was examined by crossing the Rx-Cre mice to a CAG-tdTomato reporter mouse. At the indicated ages, retinas were isolated and reporter (tdTomato) expression was analyzed. In brief, mice were transcardially perfused and tissues were fixed in 4% paraformaldehyde (PFA) overnight. Retinas were isolated and cryoprotected overnight in 30% sucrose in 1xPBS and then sectioned at 14 μm on a cryostat (Leica CM 3050S). After blocking with 10% normal donkey serum in PBS containing 0.01% Triton X-100 overnight at 4°C, retinal sections were incubated in goat antibodies against Brn3b (1:400; Santa Cruz Biotechnology, SC31989), CHAT (1:400; Millipore AB144P), Calretinin (1:400; Millipore AB1550) and TH (1:400; Millipore AB1542) in blocking solution at 4°C for 48 hrs. Retinal sections were then washed three times with 1x PBS, and incubated with donkey anti-goat secondary antibody conjugated with Alexa Fluor 488 (1:200) overnight at 4°C. After rigorous washing three times in 1x PBS, retinal sections were mounted with Fluromount-G and fluorescent images were collected using a Zeiss Axio Imager Z2 equipped with a CCD camera (AxioCam HRC, Carl Zeiss).

Quantitative RT-PCR

Quantitative RT-PCR was performed to confirm tissue specific loss of β2 subunits in Rx-β2cKOs. Retinal and collicular tissue was microdissected from P6-7 animals. Tissue was homogenized in Trizol reagent (15596-018; Invitrogen), and total RNA was isolated by using chloroform phase separation followed by precipitation with 75% alcohol and resuspended in water. cDNA was synthesized with a QuantiTect Reverse Transcription Kit (205311; Qiagen, Valencia, CA). Quantitative PCR was performed with an iQ SYBR Green Supermix Kit (170-8880; Bio-Rad, Hercules, CA) for β2 and β-tubulin, used for normalization, with an iCycler system (170-8740; Bio-Rad). Quantification was performed as previously described by Schmittgen and Livak (Schmittgen and Livak 2008; Dhande et al. 2012).

In vivo imaging of spontaneous retinal activity and data analysis

AAV virus encoding GCaMP6 was injected into eyes at P0 and spontaneous retinal activity was recorded from axonal terminals of infected RGCs at P5-6 from superior colliculus. The

procedure of surgery and imaging has been described in detail previously (Ackman et al., 2012; Burbridge et al., 2014). In brief, mice aged P5-6 were deeply anaesthetized with isoflurane (2.5-3.5%) in oxygen and then placed on a heating pad set to 37 C° using a homoeothermic temperature monitor (NPI TC-20, ALAScientific). Carprofen (Rimadyl, Pfizer, 50 mg/ml) was injected subcutaneously to induce general analgesia, and local anaesthesia was produced by subcutaneous injections of a mixture of 0.4% Marcaine and 0.4% Lidocaine (bupivacaine HCL, Hospira and Lidocaine Injectable, Sparhawk Laboratories Inc.) under the scalp. After removal of the scalp, steel head posts were fixed to the anterior and posterior portions of the exposed skull using vet-bond and cyanoacrylate glue and a craniotomy window was made for the exposure of SC. Isoflurane anaesthesia was adjusted during surgery as necessary to maintain a stable respiration rate. *In vivo* calcium imaging was conducted through the craniotomy window after a 1-2 hour recovery from isoflurane anaesthesia and the surgical procedure. Spontaneous wave activity was recorded from the SC under a 2.5x objective and image frames containing both SC hemispheres were acquired at a rate of 5 Hz. Epifluorescent illumination was provided by a mercury light source (X-Cite Series 120, EXFO) through a neutral-density filter and a filter-cube set (U-MGFPHQ, Olympus) with the minimum illumination intensity that still gave detectable calcium signals using a CCD exposure of 200 ms. A CCD camera (Pixelfly, The COOKE Corporation) coupled to an Olympus BX51 was used to image calcium responses.

Calcium-signal detection and image processing of spontaneous wave activity was carried out using custom software routines written in MATLAB (Mathworks), which has been described in detail previously (Ackman et al., 2012). Briefly, rectangular grid of ROIs (for each ROI; h=45 mm, w=45 mm) was masked over the average image, F_0, of visible calcium indicator fluorescence for each movie. Calcium signals for each ROI was the average fluorescence intensity inside each ROI in each frame, F_t, measured as a function of time ($DF/F = (F_t-F_0)/F_0$). Calcium transients were detected using automatic unbiased detection routines to identify local maxima (> 2 standard deviations of the derivative of the signal). A wave-form representing the population activity for each movie was constructed by smoothing the envelope of the population activity histogram for each movie with a 10-order Hanning filter (Hann window function in MATLAB). Local maxima separated by greater than 10 s and having rising phase onsets surpassing a 5% population activity threshold from the local minima were set as wave peak and onset times, respectively. The time between the wave peak and the next local minima when population activity during the falling phase decreased to less than 20% was set as the wave offset. Each wave period was then interactively confirmed based on the visually detected waves in the raw movie data. Any detected calcium transients occurring outside of wave periods were excluded from further analysis. The wave area was the sum of non-zero areas within the merged wave. Wave frequencies for each recording were calculated as the number of waves divided by the length of time for each recording. Inter-wave intervals for each recording were calculated as the set of time intervals between the onsets of sequential waves in each recording. Pixel intensity within each wave period was normalized and pixel numbers above threshold at 0.1-0.9 were calculated, with wave peak correlation index equaling pixel numbers at wave peak divided by the total number of pixels activated throughout each wave.

In vitro calcium imaging and data analysis

Fluorescence measurements were made in a light-proof Faraday cage, with a two-photon microscope system (Ultima, Prairie Technologies, Middleton, WI) configured on an Olympus upright microscope (BX51WI, Olympus USA, New York) with a 60×, 1.0 NA objective (LUMPlanFL/IR, Olympus) and a Ti:Sapphire pulsed laser (MaiTai, Newport, CA) tuned to 910-920 nm. Image acquisition was controlled by the Prairie software (Prairie View, Prairie Technologies). Fluorescence signals were detected simultaneously by two photomultiplier tubes at 520 ± 18 nm (green channel, bandpass filter: Semrock, FF01-520/35-25) and 607 ± 23 nm wavelength (red channel, bandpass filter: Chroma, HQ607/45), respectively. Fluorescence signals from regions (128×128 pixels, ~200×200 μm^2) of the image field containing GCaMP6-expressing ganglion cell somas were recorded in the green channel with frame period of 0.186s. For the detection of calcium events, low-pass and top-hat filtering were used to smooth and remove slow baseline drifts in the raw calcium signal traces. The filtered traces were used to detect significant change of calcium signals, i.e. calcium events, defined by amplitude > mean+2SD. Event intervals were calculated based on the peak time of each event. dF/F amplitudes for each event were calculated based on the mean of the low-pass filtered baseline 10-2s preceding the peak of each event.

Multielectrode array recording and data analysis

Spiking retinal activity was recorded *in vitro* at P4 using a multielectrode array at 34°C in Ringers containing (in mM): NaCl 124, KCl 2.5, $CaCl_2$ 2, $MgCl_2$ 2, NaH_2PO_2 1.25, NaHCO3 26, and glucose 22 (pH 7.35 and oxygenated with 95% O_2 and 5% CO_2). Action potentials were simultaneously recorded from 60 electrodes spaced 100μm apart. The signals were filtered between 100 Hz and 3 kHz. Offline data analysis was carried out using Offline Sorter (Plexon, Dallas, TX), NeuroExplorer (Nex Technologies, Lexington, MA) and a custom program. A number of retinal wave properties were measured, including firing rate, correlation index, wave frequency and wave size. Firing rate was calculated either by spiking frequency during the whole recording period or during a particular wave, where appropriate.

The spike time tiling coefficient (STTC), a measure of correlated activity between cells, was calculated as previously described (Cutts and Eglen, 2014). Briefly, it was determined by calculating the number of spikes from cell A that fall within a specified time window of a spike from cell B. $STTC = (1/2)((P_A-T_B)/(1-P_AT_B)+(P_B-T_A)/(1-P_BT_A))$ where P_A = the proportion of spikes from cell A which lie within $\pm\Delta t$ of any spike from cell B, and vice versa for P_B; T_A = the proportion of total recording time which lies within $\pm\Delta t$ of any spike from A, and vice versa for T_B (Cutts and Eglen, 2014). The STTC “Random” base line was calculated from random shuffling of the cKO and cHet MEA data sets used for calculating the STTC. All spike times recorded from one electrode were shifted by adding the same random time to each spike while keeping the same starting and ending time. Different electrodes were shifted with different random values.

Burst analysis was performed using the Surprise algorithm provided by NeuroExplorer (Nex Technhnologies, Madison AL). First the mean inter-spike interval (ISI), ∂, was calculated

for the neuron and Neuroexplorer scanned the spike train until at least three spikes were found such that their mean ISI < ∂/2. The Surprise (S) of the resulting 3-spike sequence was then calculated:

$$\mathrm{S}=-log_{10}\left(\mathrm{Probability\ P\ has\ at\ least\ N\ spikes\ in\ a\ time\ interval\ of\ length\ T}\right),$$

the burst has N spikes, the time from the first to the last spike of the burst is T, and the algorithm assumes that the random variable P has a Poisson distribution. NeuroExplorer adds spikes to the end of the burst until the first ISI is more than ∂ and then calculates the Surprise for each of the bursts. The burst with maximum surprise (Smax) is then selected. If Smax is more than MinSurprise and the number of spikes in the burst is more than 3, NeuroExplorer adds the burst to the result.

Dye Injections, fluorescent images and data analysis

Focal DiI injections (2.3 nl) for measurements of retinotopy were performed, imaged and quantified as described (Xu et al., 2011). In brief, lipophilic dye 1,1′-dioctadecyl-3,3, 3′,3′-tetramethylindocarbocyanine perchlorate (DiI) (2.3 nl) was injected into the retina using a Nanoject (Drummond Scientific, Broomall, PA) to label a small group of neighbouring RGCs at the injection site. Injections were localized along the perimeter of the retina, using as a reference the insertion points of the four major eye muscles. Pups were anesthetized with a veterinary anesthetic cocktail (in mg/ml: 4.28 ketamine, 0.82 xylazine and 0.07 acepromazine) at P6. The injected pups were allowed to recover from anesthesia and then put back with their mother for 48 hours to allow transport of tracer from the retina to the SC and dLGN. Mice were sacrificed and intercardially perfused with 4% paraformaldehyde in PBS at P8.

Labelled axonal projections were imaged from SC, which was exposed by carefully removing the overlying cortex and photographed under fluorescent illumination using a CCD camera (AxioCam HRC, Carl Zeiss). Retinas of injected animals were isolated, mounted on slides using Fluoromount G (ElectroMicroscopy Science, PA) and then imaged using the same CCD camera. Image quantification was performed blind to genotype. Quantification of focal DiI injection labelled “target zones” in the colliculus followed previously published methods and was reported as the ratio of target area to total SC area (Chandrasekaran et al., 2005). Briefly, the SC was outlined manually and the area of the total SC was measured. The target area labelled by the dye injection was calculated by subtracting background fluorescence and measuring the area of the target above one half of the maximum fluorescence at the target. The retinal injection size, quantified by measuring the area of fluorescent signal in the retina above one half of the maximum fluorescent signal after background subtraction, showed no difference across all genotypes and injection locations, and there was no relationship between TZ area and retinal injection area (McLaughlin et al., 2003; Xu et al., 2011).

Measurements of eye-specific segregation were performed with whole eye injections (1 μl into the vitreous) of cholera toxin subunit B (CTB) conjugated to Alexa Fluor (Molecular Probes, OR), CTB-488 and CTB-555, into the left eye and the right eye, respectively, to

bulk label all RGCs. Injected animals were sacrificed 48 hours later and the entire brain was fixed overnight, sectioned at 150 μm either sagitally (for SC images) or coronally (for dLGN images) on a vibratome and imaged using the same CCD camera. Eye-specific segregation in the SC was quantified by measuring the fraction of fluorescence signal labelled from the ipsilateral eye in the SGS layer, where axons only from the contralateral eye usually terminate. The total SGS was outlined manually based on fluorescence signals and the fraction of the ipsilateral eye projection and overlap was calculated at the various reported thresholds. The quantification of eye-specific segregation in the dLGN followed previously published methods (Stellwagen and Shatz, 2002; Torborg and Feller, 2004; Torborg et al., 2005; Xu et al., 2011; Zhang et al., 2011). Briefly, three sections that contained the largest ipsilateral projection, corresponding to the central third of the dLGN, were selected and data were averaged across these sections. The fraction of pixels in the dLGN that contained ipsi label, contra label and both ipsi and contra label (overlapping) were calculated across a range of thresholds and reported as the 'Fraction of ipsi projection', 'Fraction of contra projection' and 'Fraction of overlap', respectively. The segregation index was calculated using methods that are threshold-independent, as described in Torborg and Feller, 2004. The intensity ratio for each pixel was computed as $R=\log_{10}(F_I/F_C)$, where F_I and F_C are fluorescence intensities from the ipsi- and contra-projection, respectively, and the variance of the R distribution, which we refer to as the "Segregation index", was calculated from these values. High R variance (Segregation index) indicates more contra-only and ipsi-only dominant pixels, and therefore more eye segregation.

Results

Decreased transcription of β2-nAChRs in retina using a Cre-loxP system

We generated mice in which the transcription of *Chrnβ2* was decreased in the retina using conditional deletion via the Cre-loxP system. We crossed mice expressing Cre in the retina but not the thalamus or midbrain driven by the Rx promoter (Swindell et al., 2006; Dhande et al., 2012) with mice in which the largest exon of the β2-nAChR is flanked by loxP sites to generate retina-specific β2-nAChR knockout mice (Rx-β2cKO). Floxed β2-nAChR mice generate functional nulls upon Cre-mediated excision (Burbridge et al., 2014), but, unfortunately, specific nAChR antibodies do not exist to confirm β2-nAChR deletion in the retina of Rx-β2cKO mice at the protein level (Moser et al., 2007; Jones and Wonnacott, 2005). Instead, we examined tdTomato expression in Rx-Cre;floxed-tdTomato mice and *Chrnb2* mRNA expression in Rx-β2cKO mice.

Cre expression in the retina begins at around E9 in Rx-Cre mice (Swindell et al., 2006). At postnatal day eighteen, Cre was strongly expressed in cells of the inner nuclear layer (INL) and the ganglion cell layer (GCL) of the retina (Fig. 1A). tdTomato was also observed in the inner plexiform layer (IPL) and the outer plexiform layer (OPL), where bipolar cells form synaptic connections with photoreceptors and RGCs, respectively. Intense tdTomato signal in cells that extend processes radially across the entire retina is likely from Müller glia, as double immunostaining showed colocalization with glial fibrillary acidic protein (GFAP) (Fig. 1B). To clarify the neuronal identity and the relative population of Cre expressing cells in the INL and GCL, we performed a series of double immunostaining experiments to label

specific cell types in retinal sections of an Rx-Cre+, tdTomato-expressing mice. Cre expressing neurons included RGCs, bipolar cells, and various amacrine cell subtypes. Quantitative analysis showed that Cre is expressed in about 85% of neurons across most neural types (Fig. 1G), including Brn3b expressing RGCs (Fig. 1C), calretinin positive amacrine cells (Fig. 1D) and Chat-positive amacrine cells (Fig. 1E). However, we found only 31% (6 out of 19) of dopaminergic amacrine cells expressed Cre (Fig. 1F) in Rx-Cre mice. As $Chat^{+}$ amacrine cells and $Brn3b^{+}$ RGCs are known to be necessary for acetylcholine retinal wave initiation and transmission, Rx-Cre mediated knockout of β2-nAChR subunits likely results in the functional disruption of waves during the first postnatal week.

Retina-specific deletion of *Chrnb2* was achieved by crossing Rx-Cre mice with floxed–β2 mice (Rx-β2cKO, Fig. 1H). To test the efficiency of Cre-dependent DNA recombination, we performed real-time PCR at postnatal day six and found that transcription of *Chrnb2* in the retina of Rx-β2cKO mice was 10 fold less than in wild type mice. As a control, we examined the transcription of *Chrnb2* in the superior colliculus (SC), where Cre expression was not observed in Rx-Cre mice, and found comparable levels of Chrnb2 mRNA between Rx-β2cKOs and wild type mice (Fig. 1I). This confirms that there was substantial deletion of *Chrnb2* mRNA in the retina of Rx-β2cKO mice, but that collicular targets of RGCs maintain their expression of β2-nAChRs.

Spontaneous retinal activity is altered, truncated in Rx-β2cKOs

To determine whether spontaneous retinal activity was affected by reduced β2-nAChR expression, we examined spontaneous activity in retinal ganglion cells *in vivo* during the first postnatal week (P3-P6) by loading retinal ganglion cells (RGCs) with a genetically encoded (GCaMP6) fluorescent calcium indicator. Retinal waves were imaged in topographically-mapped RGC axon arbors in the SC (Fig. 2A). The spatiotemporal properties of spontaneous wave activity was previously characterized in wild type and β2KO mice using this approach (Ackman et al., 2012; Burbridge et al., 2014). In both wild type and β2 heterozygous mice, spontaneous activity occurs periodically and propagates across the SC with a well-defined wave front (Ackman et al., 2012; Burbridge et al., 2014; **Fig. 2B** and **2C**). In mice lacking β2-nAChRs throughout their brain and body, correlated RGC activity occurs *in vivo*, but is much less frequent and of lower amplitude than WT controls. Typical spontaneous activity in β2KO mice lacks a clear wave front and encompasses the entire retina in a “flashing” rather than a “propagating” manner (Burbridge et al., 2014).

We examined spontaneous retinal activity in Rx-β2cKO and compared it to that of β2KO and heterozygous controls. Spontaneous wave activity in the Rx-β2cKOs (Fig. 2D) occurred at a lower frequency (0.36 ± 0.17 per min, Figure 2F) but with smaller amplitude (0.02 ± 0.005, Figure 2G) compared with heterozygous controls (Rx-β2cHet: Freq = 0.77 ± 0.05 per min and Amp = 0.05 ± 0.008, P = 0.07 and 0.03, respectively, compared with Rx-β2cKOs; $\beta2^{+/-}$: Freq = 0.94 ± 0.1, originally reported in Burbridge et al., 2014) and was not different from β2KO mice (β2KO Freq = 0.39 ± 0.05 P=0.89, compared with Rx-β2cKOs). “Flashing waves”, typical of β2KO mice, were also observed in Rx-β2cKO mice (Fig. 2E, indicated by blue dashed lines), along with more normal “propagating waves” that traverse the SC with

well-defined wave fronts (Figure 2D and 2E, indicated by red dashed lines), which are not observed in β2KO mice. Most "propagating" waves in Rx-β2cKO mice travel only a short distance, and therefore the average wave size and duration is much smaller (Fig. 2H, Rx-β2cKO size = 0.29mm^2 ± 0.096, Rx-β2cHet = 0.89mm^2 ± 0.016, P=0.05) (Fig. 2I**,** Rx-β2cKO duration = 6.4s ± 1, Rx-β2CHet = 27.8s ± 3.5, P<<0.001) relative to heterozygous controls. To further quantify the difference in propagation character of spontaneous retinal activity without a well-defined wave front, we calculated a combined measure of wave coverage and speed ("propagation speed") by dividing the total area covered by a wave by the total wave duration. Most waves in β2 heterozygous mice (both β2$^{+/-}$ and Rx-Cre$^+$;β2$^{flox/+}$) show a clear, slowly propagating wave front, and therefore, the propagation speed is relatively small and uniform, with a narrowly distributed peak at ~3.5×10^5 μm^2/s (Figure 2K, 2L). In β2KO mice, however, spontaneous activity is more "flashy", and the propagation speed is significantly higher than that of heterozygous controls (β2Het area/s = 5.4×10^5 μm^2/s ± 0.3×10^5, β2KO = 11.2×10^5 μm^2/s ± 0.4×10^5, P<<<0.001, Figures 2K, 2L). Interestingly, the propagation speed in Rx-β2cKO mice was quite variable, with some spontaneous waves propagating normally and others rapidly sweeping across the SC. Therefore, the propagation speed of waves forms a wider distribution with a peak similar to β2 heterozygous controls and a tail that extends to the "flashy" range typical of β2KO mice (Figures 2K, 2L). The normal "propagating" waves make up about half of total waves in the Rx-β2cKO mice (Fig. 2M). The mean propagation speed of waves in Rx-β2cKO mice was significantly smaller than that of β2KO mice (Rx-β2cKO area/s = 8.6×10^5 μm^2/s ± 1.3×10^5, P = 0.03, Fig. 2N), but was still significantly higher than in Rx-β2cHet controls (Rx-β2cHet area/s = 3.5×10^5 μm^2/s ± 2.4×10^4, P = 0.0002).

RGC activity is reduced at the single cell level in Rx-β2cKO mice

In vivo imaging of retinal waves in RGC axon terminals in the SC can not unambiguously determine whether reduced Ca^{2+} signals in Rx-β2cKO mice are the result of a reduction in RGC neuronal activity or altered RGC axon terminals. To address this, we imaged Ca^{2+} in retinal neuron cell bodies at single cell resolution in acutely isolated retinas. Rx-β2cKOs and heterozygous control (β2$^{flox/+}$; Rx-Cre$^+$) eyes were injected with virus encoding GCaMP6 at P0 and the injected retinas were isolated at P5-6. Spontaneous retinal activity was imaged using a two-photon microscope and a 60x objective lens. In heterozygotes, we observed large, periodic calcium events encompassing most neurons in the GCL that were stable across the entire recording period. Importantly, calcium transients were highly correlated, which reflects wave activity propagating across the entire recording field (Fig. 3A). In contrast, single cell calcium transients in Rx-β2cKO mice were weak, fluctuated with time and activity was less correlated between cells in comparison with heterozygous controls (Fig. 3B). Although calcium activity was often synchronized in Rx-β2cKO mice (indicated by black dashed lines), we also found many calcium events that were not correlated in neighboring cells (indicated by red dashed lines). On average, the amplitudes of calcium transients were significantly smaller (Fig. 3C, P < 0.001 for both K-S and student t-tests) and inter-event intervals (Fig. 3D) showed greater variation in Rx-β2cKO mice (41 cells from 2 retinas) relative to control mice (45 cells from 2 retinas). Interestingly, despite the irregularity of the calcium events, the mean interevent interval observed in the Rx-β2cKOs was not different from heterozygous control retinas (Fig. 3D inset, P>0.05, student t-test).

We also directly recorded spiking activity in RGCs using a multielectrode array system in retinas acutely isolated from both Rx-β2cKO and control mice. RGCs in control WT ($\beta2^{flox/+;}$ Rx-Cre^{-}) and heterozygous ($\beta2^{flox/+}$; Rx-Cre^{+}) mice exhibited highly correlated, periodic bursting activity as is typically observed during a retinal wave (Fig. 4A). Although bursting activity was also found in Rx-β2cKO mice (Fig. 4A), burst frequency was significantly reduced in comparison to controls (Fig. 4E) and the number of spikes in each burst was much less when compared with WT control mice (Fig. 4G), which results in a large reduction in the overall firing rate in Rx-β2cKO mice (Fig. 4C). On average, the firing rate in Rx-β2cKOs was reduced to only ~25% of wild type control mice. The activity that remained in Rx-β2cKOs was mediated by residual β2-nAChRs, as it was completely abolished by the application of DHβE, a selective antagonist of β2-containing nAChRs, suggesting an incomplete deletion of β2 subunits in Rx-β2cKO retinas (Fig. 4C). We also examined the correlation in RGC activity as a function of distance (separation) by computing a correlation index. Since overall firing rates are significantly lower in Rx-β2cKO mice, it is important to control for firing rate, so we chose a 'spike time tiling coefficient' (STTC), introduced by Cutts and Eglen (2014) to measure activity correlations without contamination by differences in firing rate. We found that activity was much less correlated overall in Rx-β2cKO mice relative to control mice (Fig. 4B). Although large propagating waves were occasionally observed in the Rx-β2cKO mice, much of the bursting activity was outside of these waves and as a consequence, RGC spiking activity in Rx-β2cKO mice was significantly less correlated over long distances relative to control mice (Fig. 4B). However, nearby RGCs were still highly correlated compared to what would be expected by chance (**Fig. 4A** and **4B**), which is consistent with the *in vivo* observation that many small waves propagated locally in in Rx-β2cKO mice (Fig. 2). Overall, results from the *in vitro* Ca^{2+} imaging and multielectrode array experiments were similar, and together with the *in vivo* Ca^{2+} imaging data suggest a reduction in overall wave fidelity in Rx-β2cKO mice, with RGCs firing more irregularly and less frequently in Rx-β2cKO mice in comparison to control mice.

Eye specific segregation is disrupted in the Rx-β2cKO mice

The development of eye-specific segregation is critically dependent on spontaneous retinal activity and can be interrupted by either blockade or disruption of spatiotemporal patterns of spontaneous retinal activity (Kalil et al., 1986; Huberman et al., 2008; Xu et al., 2011; Zhang et al., 2011, Burbridge et al., 2014). To determine whether the development of eye-specific segregation is affected in Rx-β2cKO mice, we filled each eye with separate fluorescent dyes and RGC axonal projections were examined in both the dorsal lateral geniculate nucleus (dLGN) and superior colliculus (SC). In wild type ($\beta2^{flox/+}$, Rx-Cre^{-}) and heterozygous ($\beta2^{flox/+}$, Rx-Cre^{+} and $\beta2^{flox/-}$, Rx-Cre^{-}) mice, RGC projections from the two eyes are well segregated in the dLGN, with axons from the contralateral eye surrounding a small zone of exclusively ipsilateral projections. In Rx-β2cKO mice, in contrast, ipsilateral RGC axons projected to a significantly enlarged area in the dLGN and abnormally overlapped with axonal projections from the contralateral eye (**Fig. 5A** and **5B**), suggesting a disruption in eye-specific segregation. Eye-specific projections to the SC also appeared disrupted in Rx-β2cKO mice. RGC axons from each eye normally project to distinct layers in the SC, with axons from the contralateral eye terminating in the most superficial layer, the

stratum griseum superficiale (SGS), and axons from the ipsilateral eye terminating in a slightly deeper layer, the stratum opticum (SO) (Dräger and Olsen, 1980). However, in Rx-β2cKOs, a significant portion of ipsilateral axons projected to the superficial layer and overlapped with projections from the contralateral eye (**Fig. 5C** and **5D**), consistent with a general disruption in eye-specific segregation in Rx-β2cKO mice.

Normal retinotopic refinement in Rx-β2cKO mice

Despite similar and low overall activity levels during the first postnatal week, the spatiotemporal properties of retinal waves were dramatically different between Rx-β2cKO and β2KO mice. Most waves in Rx-β2cKOs demonstrated typical “propagating” features, rather than the rapid “flashing” characteristics of waves observed in β2KO mice (Burbridge et al., 2014). To examine whether the spatiotemporal features of propagating waves contributed to the refinement of RGC axonal arbors, we examined the development of retinotopy in Rx-β2cKOs in comparison to WT and β2KO mice. Retinotopic development was assessed using focal DiI injections in the retina and quantification of RGC target zone size in the SC. In both WT and heterozygous mice, axons from a local group of RGCs arborize in a small target zone in the SC. Complete genetic deletion of β2-nAChRs results in a dramatic enlargement of RGC target territory (Grubb et al., 2003; McLaughlin et al., 2003; Xu at al., 2011), which is the specific result of deleting β2-nAChRs from the retina (Burbridge et al., 2014). In Rx-β2cKO mice, RGCs from the dorsal retina innervated a restricted area in the SC that was comparable to that observed in WT and heterozygous control mice, suggesting that RGC axon projections from the dorsal retina developed normally in Rx-β2cKO mice (**Fig. 6A top** and **6B**).

In contrast, the refinement of ventral-temporal RGC axon projections to the SC was significantly disrupted in Rx-β2cKOs (**Fig. 6A middle** and **6C**), and comparable to those observed in whole animal β2KO mice. Due to the lateral position of their eyes, binocular projections in mice are limited to the ventral-temporal retina. The ventral-temporal RGC axon refinement failures observed in Rx-β2cKO mice may be a consequence of disrupted eye-specific segregation. In other words, RGCs that fail to segregate with respect to eye of origin may also consequently lack retinotopic refinement. To test this possibility, we eliminated eye competition by enucleating one eye at birth. Remarkably, ventral-temporal RGC axon refinement was normal in Rx-β2cKO mice following monocular enucleation (**Fig. 6A** bottom and **6D**), consistent with what was previously observed in β2(TG) mice (Xu et al., 2011), suggesting that abnormal retinotopic refinement in Rx-β2cKO mice is a direct consequence of disrupted eye segregation.

We performed similar anatomical studies to examine the development of retinotopy in the dLGN. Consistent with retinocollicular development, RGC projections from the dorsal retina developed normally in the dLGN of Rx-β2cKO mice. In contrast, RGCs from the ventral-temporal retina of Rx-β2cKO mice arborized in an abnormally large territory in the dLGN when compared with wild type control mice ($P < 0.001$). However, axons from ventral-temporal RGCs refined normally in Rx-β2cKO mice following monocular enucleation (Fig. 7A and 7B). These results again suggest that RGCs throughout the retina of Rx-β2cKO mice are capable of normal retinotopic refinement mediated by the small

propagating waves observed in Rx-β2cKO mice, even though overall retinal activity levels are significantly reduced in these mutant mice.

Truncated retinal waves in β2(TG) mice

Curiously, RGC projection patterns in Rx-β2cKO mice were very similar to those previously observed in β2(TG) mice (Xu et al., 2011). In particular, eye-specific segregation is disrupted in β2(TG) mice, whereas retinotopic map refinement is normal so long as eye competition is eliminated by monocular enucleation. We examined and characterized the features of retinal waves *in vivo* in β2(TG) mice to further understand the role of propagating retinal waves in retinotopic refinement. We previously reported using *in vitro* multielectrode array techniques that RGCs in β2(TG) mice fire at levels indistinguishable from WT control mice, but that β2(TG) mice have truncated ('small') retinal waves due to the incomplete restoration ('rescue') of β2-nAChRs in the retina (Xu et al., 2011). Consistent with our previous *in vitro* findings, waves observed *in vivo* in β2(TG) mice were smaller (**Fig. 8A** and **8B,** β2(TG) wave size= 5.0×10^5 um^2 ± 0.7×10^5, β2Het = 9.8×10^5 ± 0.6×10^5, P=0.002) and briefer (Fig. 8C**,** β2(TG) wave duration = 14.0s ± 4.0, Rx-β2cHet = 21.3 ± 1.2, P=0.04) than waves in control mice. Activity levels, measured through ROI activation frequency, were also not statistically different in β2(TG) mice compared to β2 heterozygous controls (Fig. 8E**,** β2(TG) frequency = 0.60 ± 0.13, β2Het = 0.88 ± 0.07, P=0.27). Despite their significantly smaller size, waves in β2(TG) mice displayed a clear wave front and propagated (area/duration) in a similar manner to those in β2 heterozygous controls (Fig. 8G-I**,** β2(TG) = 4.3×10^4 $\mu m^2/s$ ±0.7, β2Het = 5.3×10^4 ± 0.3, P=0.54), without obvious "flashing" activity, typical of β2KO mice. These results suggest that local, small propagating retinal waves, despite a significant reduction in overall activity levels, were sufficient to mediate retinotopic refinement in the absence of binocular competition in both β2(TG) and Rx-β2cKO mice.

Discussion

We aimed to clarify the relative roles of overall activity levels and spatiotemporal patterns of retinal activity in the development of visual maps. We achieved the desired manipulation by altering the transcription of retinal β2-nAChRs using a Cre-loxP system, with transcription of β2-nAChRs in the retina of Rx-β2cKO mice reduced 10-fold, but midbrain β2-nAChR expression unaffected. Conditional deletion of β2-nAChRs from the retina decreased retinal activity in Rx-β2cKO mice to a level comparable to that observed in whole-animal β2KO mice *in vivo*. However, the spatiotemporal pattern of spontaneous activity in Rx-β2cKO mice, examined both *in vitro* and *in vivo*, was notably different from that observed in β2KO mice. While waves in β2KO mice lack well-defined wave fronts and an obvious propagation pattern (Burbridge et al., 2014), waves in Rx-β2cKO mice frequently propagate across the SC in a manner similar to that observed WT mice. Furthermore, eye-specific segregation was completely disrupted in Rx-β2cKO mice, but retinotopic map refinement was unchanged so long as binocular competition was eliminated by monocular enucleation. These results suggest that a minimum, low level of activity and local spatial correlations in spontaneous RGC activity are necessary for retinotopic map refinement.

Role of retinal waves in visual map development: Permissive or Instructive?

Neuronal activity appears to be generated autonomously across a variety of developing brain areas and seems essential for some aspects of neural circuit development (Kirkby et al., 2013). This early neuronal activity may be *permissive* for brain development, acting in a passive way to promote gene expression, cell survival and neurite outgrowth, or *instructive* for brain development, by actively guiding circuit formation through specific spatiotemporal patterns of neural activity (Crair, 1999). However, selectively manipulating neuronal activity levels relative to activity patterns is experimentally difficult, and thus distinguishing between a permissive and instructive role for activity in brain development has been particularly challenging. In the developing visual system, RGCs fire correlated waves of activity that propagate into and through the brain and play an important role in the formation of visual maps (Meister et al., 1996; Ackman et al., 2012; Burbridge et al., 2014). Completely blocking spontaneous retinal activity profoundly disrupts both eye-specific segregation and retinotopic map refinement (Shatz and Stryker, 1988; Stretavan, Shatz and Stryker, 1988). However, manipulations that change the spatiotemporal pattern of retinal activity also typically alter RGC activity levels (McLaughlin et al., 2003; Grubb et al., 2003; Mrsic-Flogel et al., 2005; Chandrasekaran et al., 2005; Burbridge et al., 2014), making it difficult to distinguish between an instructive and a permissive role for spontaneous retinal activity.

Comparing spontaneous retinal activity in β2KO, Rx-β2CKO and β2(TG) mice

β2-nAChR expression in the retina has been genetically manipulated in several different ways, with correspondingly diverse effects on spontaneous retinal activity (Table 1). Whole animal β2KO mice lack expression of any β2-nAChRs, and RGC activity levels and retinal waves are severely perturbed *in vivo* (Burbridge et al., 2014), though there are some inconsistencies about activity levels between various *in vitro* reports (Bansal et al., 2000; Sun et al., 2008; Stafford et al., 2009). β2(TG) mice, which have β2-nAChR expression confined to the ganglion cell layer but missing elsewhere in the retina and brain, have normal levels of RGC activity but truncated or ‘small’ retinal waves both *in vitro* (Xu et al., 2011) and *in vivo* (Fig. 7). Pax6α-β2cKO mice, which completely lack β2-nAChR expression in distinct zones of the retina across all layers, have no retinal activity where β2-nAChR expression is absent both *in vitro* and *in vivo* (Burbridge et al., 2014) Finally, Rx-β2cKO (Fig. 2, 3 and 4) have greatly reduced β2-nAChR expression throughout the retina, and correspondingly reduced RGC activity and truncated retinal waves both *in vitro* and *in vivo*.

Features of spontaneous retinal activity critical for eye-specific segregation

RGC projections from the eye to the brain are segregated with respect to eye of origin (Dräger and Olsen, 1980), and the development of this segregated projection pattern requires retinal activity (Shatz and Stryker, 1988; Burbridge et al., 2014). To a certain extent, the specific features of the spontaneous retinal activity necessary for the emergence of eye-specific projections have been characterized. In particular, based on both pharmacological and genetic manipulations, more globally but not strictly locally correlated activity across the retina appears necessary for eye-specific segregation, along with a minimum overall

level of activity that is close to that normally found during development (Burbridge et al., 2014; Xu et al., 2011). In Rx-β2cKO mice, retinal activity is locally but not globally correlated, like in β2(TG) mice, and eye-specific segregation is completely disrupted. In β2KO mice, activity is globally correlated and lacks a slowly propagating, local wave front, and eye-specific segregation is rescued by pharmacological manipulations that raise activity levels to near normal levels without rescuing altered retinal activity patterns (Burbridge et al., 2014). Meanwhile, synchronizing activity in both eyes optogenetically disrupts eye-specific segregation (Zhang et al., 2011). In total, these experiments suggest that a minimum level of activity not too far below that found normally in the retina, along with correlated activity amongst RGCs across large swathes of the retina, but not between retinas, are necessary for the emergence of eye-specific segregation.

Features of spontaneous retinal activity critical for retinotopic refinement

The development of refined retinotopic projections from the eye to the brain appears to be dependent on distinct and different features of spontaneous retinal activity than eye-specific projections. First, spontaneous activity that is correlated globally and locally to a similar degree appears to interfere with retinotopic refinement. In other words, the presence of waves with a distinct wave front that propagates slowly across the retina and produces local correlations in activity between RGCs that are much stronger than global (long distance) correlations, appears necessary for normal retinotopic refinement. Globally correlated activity, like that in β2KO mice (Burbridge et al., 2014) or mice that are optogenetically manipulated (Zhang et al., 2011), disrupts retinotopic refinement. However, retinotopic refinement does not appear to be particularly sensitive to overall levels of retinal activity. Even activity levels dramatically reduced below the norm, as in Rx-β2cKO, can produce normal retinotopic refinement as long as the activity is strongly correlated locally between nearby RGCs. Consistent with this, raising activity levels pharmacologically to near normal levels in β2KO mice is sufficient to rescue eye-specific segregation but not retinotopic refinement, likely because the ‘rescued’ activity in β2KO mice does not consist of locally correlated propagating wave fronts. Thus, it appears that retinotopic refinement and eye-specific segregation are differentially sensitive to both overall activity levels and correlations in the activity amongst RGCs.

Binocular competition disrupts retinotopy in multiple retinal wave knockouts

It is notable, and quite remarkable, that retinotopic refinement in ventral-temporal (‘binocular zone’) RGCs in Rx-β2cKO is normal only when competition between the two eyes is removed by monocular enucleation (Fig. 6). In other (monocular) zones of the retina, retinotopic refinement appears normal, even while eye-specific segregation is completely disrupted. The interdependence of retinotopic refinement on eye-specific segregation observed in Rx-β2cKO mice is very similar to that noted in β2(TG) mice (Xu et al., 2011), and serves as an important reminder that it is the same RGC axons that must simultaneously map with respect to eye of origin and retinotopy in the binocular portions of the retina. Despite the fact that the development of refined retinotopy and eye-specific segregation are interdependent, each map is sensitive to distinct features of spontaneous retinal activity, including overall activity levels and RGC correlations.

Summary

In Table 1, we offer a comparison of retinal activity and visual map phenotypes across the various strains of genetically manipulated β2-nAChR mice. Previously, using β2(TG) mice (Xu et al., 2011), we provided evidence to show that reducing the spatial extent of waves (their 'size') disrupted eye-specific segregation without interfering with retinotopy (so long as competition between the eyes was removed by monocular enucleation). Overall levels of retinal activity in β2(TG) mice are not altered in comparison to WT mice. This data demonstrated that merely the presence of normal levels of spontaneous activity is not sufficient to promote eye-specific segregation. Rather, eye-specific segregation is sensitively dependent on the pattern of spontaneous activity, and 'large' waves with correlations amongst retinal ganglion cells across long distances are necessary for normal segregation. Here, we used an additional manipulation of β2-nAChR expression (the Rx-β2cKO mice) to examine the relationship between retinal activity and visual map development. In Rx-β2cKO mice, retinal activity levels are very substantially reduced in comparison to control and β2(TG) mice. Retinal waves are also altered, with some 'small' and normally propagating waves, like in β2(TG) mice (Xu et al., 2011), along with some 'flashy' waves, similar to those observed in β2KO mice (Burbridge et al., 2014). Overall retinal activity levels in Rx-β2cKO mice were reduced to a level comparable to that seen in β2KO mice *in vivo*. Despite the dramatic reduction in retinal activity levels, the overall anatomical phenotype in Rx-β2cKO mice was indistinguishable from that observed in β2(TG) mice, with normal retinotopy (in the absence of between eye competition), but disrupted eye segregation. In summary, given the anatomical and physiological (*in vivo* and *in vitro*) phenotype of the Rx-β2cKO mice described here, we infer that even low levels of local (but not long-distance or 'global') correlated activity are sufficient to promote retinotopic refinement. However, the absence of long-range correlations in RGC activity in Rx-β2cKO and β2(TG) mice prevent the emergence of normal eye-specific segregation. It remains an open question and important future area of investigation to elucidate precisely what cellular and molecular mechanisms are responsible for translating distinct features of spontaneous retinal activity into refined and accurate maps of the visual world.

References

1. Ackman JB, Burbridge TJ, Crair MC. Retinal waves coordinate patterned activity throughout the developing visual system. Nature. 2012; 490:219–225. [PubMed: 23060192]
2. Ackman JB, Crair MC. Role of emergent neural activity in visual map development. Curr Opin Neurobiol. 2014; 24:166–175. [PubMed: 24492092]
3. Bansal A, Singer JH, Hwang BJ, Xu W, Beaudet A, Feller MB. Mice lacking specific nicotinic acetylcholine receptor subunits exhibit dramatically altered spontaneous activity patterns and reveal a limited role for retinal waves in forming ON and OFF circuits in the inner retina. J. Neurosci. 2000; 20:7672–81. [PubMed: 11027228]
4. Blankenship AG, Feller MB. Mechanisms underlying spontaneous patterned activity in developing neural circuits. Nat Rev Neurosci. 2010; 11:18–29. [PubMed: 19953103]
5. Burbridge TJ, Xu HP, Ackman JB, Ge X, Zhang y. Ye MJ, Zhou ZJ, Xu J, Contractor A, Crair MC. Visual circuit development requires patterned activity mediated by retinal acetylcholine receptors. Neuron. 2014; 84(5):1049–64. [PubMed: 25466916]
6. Chalupa LM. Retinal waves are unlikely to instruct the formation of eye-specific retinogeniculate projections. Neural Dev. 2009; 4:25. [PubMed: 19580684]

7. Chandrasekaran AR, Plas DT, Gonzalez E, Crair MC. Evidence for an instructive role of retinal activity in retinotopic map refinement in the superior colliculus of the mouse. J. Neurosci. 2005; 25:6929–6938. [PubMed: 16033903]
8. Cline H. Sperry and Hebb: oil and vinegar? Trends Neurosci. 2003; 26:655–661. [PubMed: 14624849]
9. Crair MC. Neuronal activity during development: permissive or instructive? Curr. Opin. Neurobiol. 1999; 9:88–93. [PubMed: 10072369]
10. Del Rio T, Feller MB. Early retinal activity and visual circuit development. Neuron. 2006; 52:221–222. [PubMed: 17046683]
11. Demas J, Sagdullaev BT, Green E, Jaubert-Miazza L, McCall MA, Gregg RG, Wong RO, Guido W. Failure to maintain eye-specific segregation in nob, a mutant with abnormally patterned retinal activity. Neuron. 2006; 50:247–259. [PubMed: 16630836]
12. Dhande OS, Bhatt S, Anishchenko A, Elstrott J, Iwasato T, Swindell EC, Xu HP, Jamrich M, Itohara S, Feller MB, Crair MC. Role of adenylate cyclase 1 in retinofugal map development. J Comp Neurol. 2012; 520:1562–1583. [PubMed: 22102330]
13. Dräger UC, Olsen JF. Origins of crossed and uncrossed retinal projections in pigmented and albino mice. J. Comp. Neurol. 1980; 191:383–412. [PubMed: 7410600]
14. Feldheim DA, O'Leary DD. Visual map development: bidirectional signaling, bifunctional guidance molecules, and competition. Cold Spring Harb. Perspect. Biol. 2010; 2:a001768. [PubMed: 20880989]
15. Feller MB. Spontaneous correlated activity in developing neural circuits. Neuron. 1999; 22:653–656. [PubMed: 10230785]
16. Feller MB. Retinal waves are likely to instruct the formation of eye specific retinogeniculate projections. Neural Dev. 2009; 4:24. [PubMed: 19580682]
17. Feller MB, Wellis DP, Stellwagen D, Werblin FS, Shatz CJ. Requirement for cholinergic synaptic transmission in the propagation of spontaneous retinal waves. Science. 1996; 272:1182–1187. [PubMed: 8638165]
18. Firth SI, Wang CT, Feller MB. Retinal waves: mechanisms and function in visual system development. Cell Calcium. 2005; 37:425–432. [PubMed: 15820390]
19. Godement P, Salaün J, Imbert M. Prenatal and postnatal development of retinogeniculate and retinocollicular projections in the mouse. J. Comp. Neurol. 1984; 230:552–575. [PubMed: 6520251]
20. Grubb MS, Rossi FM, Changeux JP, Thompson ID. Abnormal functional organization in the dorsal lateral geniculate nucleus of mice lacking the beta 2 subunit of the nicotinic acetylcholine receptor. Neuron. Dec 18; 2003 40(6):1161–72. 2003. [PubMed: 14687550]
21. Huberman AD, Feller MB, Chapman B. Mechanisms underlying development of visual maps and receptive fields. Annu. Rev. Neurosci. 2008; 31:479–509. [PubMed: 18558864]
22. Jones IW, Wonnacott S. Why doesn't nicotinic Ach receptor immunoreactivity knock out? Trend Neurosci. 2005; 28:343–345. [PubMed: 15979499]
23. Kalil RE, Dubin MW, Scott G, Stark LA. Elimination of action potentials blocks the structural development of retinogeniculate synapses. Nature. 1986; 323:156–158. [PubMed: 3018590]
24. Kirkby LA, Sack GS, Firl A, Feller MB. A role for correlated spontaneous activity in the assembly of neural circuits. Neuron. 2013; 80:1129–144. [PubMed: 24314725]
25. McLaughlin T, O'Leary DDM. Molecular gradients and development of retinotopic maps. Annu. Rev. Neurosci. 2005; 28:327–355. [PubMed: 16022599]
26. McLaughlin T, Torborg CL, Feller MB, O'Leary DD. Retinotopic map refinement requires spontaneous retinal waves during a brief critical period of development. Neuron. 2003; 40:1147–1160. [PubMed: 14687549]
27. Meister M, Wong ROL, Baylor DA, Shatz CJ. Synchronous bursts of action potentials in ganglion cells of the developing mammalian retina. Science. 1991; 252:939–943. [PubMed: 2035024]
28. Moser N, Mechawar N, Jones I, Gochberg-Sarver A, Orr-Urtreger A, Plomann M, Salas R, Molles B, Marubio L, Roth U, Maskos U, Winzer-Serhan U, Bourgeois JP, Le Sourd AM, De Biasi M, Schröder H, Lindstrom J, Maelicke A, Changeux JP, Wevers A. Evaluating the suitability of

nicotinic acetylcholine receptor antibodies for standard immunodetection procedures. J Neurochem. 2007; 102:479–92. [PubMed: 17419810]

29. Mrsic-Flogel TD, Hofer SB, Creutzfeldt C, Cloëz-Tayarani I, Changeux JP, Bonhoeffer T, Hübener M. Altered map of visual space in the superior colliculus of mice lacking early retinal waves. J Neurosci. 2005; 25:6921–6928. [PubMed: 16033902]
30. Penn AA, Riquelme PA, Feller MB, Shatz CJ. Competition in retinogeniculate patterning driven by spontaneous activity. Science. 1998; 279:2108–2112. [PubMed: 9516112]
31. Sanes JR, Zipursky SL. Design principles of insect and vertebrate visual systems. Neuron. 2010; 66:15–36. [PubMed: 20399726]
32. Schmittgen TD, Livak KJ. Analyzing real-time PCR data by the comparative CT method. Nat Protoc. 2008; 3:1101–1108. [PubMed: 18546601]
33. Shatz CJ, Stryker MP. Prenatal tetrodotoxin infusion blocks segregation of retinogeniculate afferents. Science. 1988; 242:87–89. [PubMed: 3175636]
34. Sretavan DW, Shatz CJ, Stryker MP. Modification of retinal ganglion cell axon morphology by prenatal infusion of tetrodotoxin. Nature. 1988; 336:468–471. [PubMed: 2461517]
35. Stafford BK, Sher A, Litke AM, Feldheim DA. Spatial-temporal patterns of retinal waves underlying activity-dependent refinement of retinofugal projections. Neuron. 2009; 64:200–212. [PubMed: 19874788]
36. Stellwagen D, Shatz CJ. An instructive role for retinal waves in the development of retinogeniculate connectivity. Neuron. 2002; 33:357–367. [PubMed: 11832224]
37. Sun C, Warland DK, Ballesteros JM, van der List D, Chalupa LM. Retinal waves in mice lacking the beta2 subunit of the nicotinic acetylcholine receptor. Proc Natl Acad Sci U S A. 2008; 105:13638–13643. [PubMed: 18757739]
38. Swindell EC, Bailey TJ, Loosli F, Liu C, Amaya-Manzanares F, Mahon KA, Wittbrodt J, Jamrich M. Rx-Cre, a tool for inactivation of gene expression in the developing retina. Genesis. 2006; 44:361–363. [PubMed: 16850473]
39. Tootell RB, Silverman MS, Switkes E, De Valois RL. Deoxyglucose Analysis of Retinotopic Organization in Primate Striate Cortex. Science. 1982; 218:902–904. [PubMed: 7134981]
40. Torborg CL, Feller MB. Unbiased analysis of bulk axonal segregation patterns. Journal of neuroscience methods. 2004; 135(1):17–26. [PubMed: 15020085]
41. Torborg CL, Feller MB. Spontaneous patterned retinal activity and the refinement of retinal projections. Prog Neurobiol. 2005; 76:213–235. [PubMed: 16280194]
42. Torborg CL, Hansen KA, Feller MB. High frequency, synchronized bursting drives eye-specific segregation of retinogeniculate projections. Nat Neurosci. 2005; 8:72–78. [PubMed: 15608630]
43. Triplett JW, Pfeiffenberger C, Yamada J, Stafford BK, Sweeney NT, Litke AM, Sher A, Koulakov AA, Feldheim DA. Competition is a driving force in topographic mapping. Proc Natl Acad Sci U S A. 2011; 108:19060–19065. [PubMed: 22065784]
44. Wong RO. Retinal waves and visual system development. Annu Rev Neurosci. 1999; 22:29–47. [PubMed: 10202531]
45. Xu HP, Furman M, Mineur YS, Chen H, King SL, Zenisek D, Zhou ZJ, Butts DA, Tian N, Picciotto MR, Crair MC. An instructive role for patterned spontaneous retinal activity in mouse visual map development. Neuron:. 2011; 70:1115–1127. [PubMed: 21689598]
46. Xu W, Orr-Urtreger A, Nigro F, Gelber S, Sutcliffe CB, Armstrong D, Patrick JW, Role LW, Beaudet AL, De Biasi M. Multiorgan autonomic dysfunction in mice lacking the β2 and the β4 subunits of neuronal nicotinic acetylcholine receptors. The Journal of neuroscience. 1999; 19(21): 9298–9305. [PubMed: 10531434]
47. Zhang J, Ackman JB, Xu HP, Crair MC. Visual map development depends on the temporal pattern of binocular activity in mice. Nat Neurosci. 2011; 15:298–307. [PubMed: 22179110]
48. Zheng J, Lee S, Zhou ZJ. A transient network of intrinsically bursting starburst cells underlies the generation of retinal waves. Nat. Neurosci. 2006; 9:363–371. [PubMed: 16462736]
49. Zhou ZJ. Direct participation of starburst amacrine cells in spontaneous rhythmic activities in the developing mammalian retina. J Neurosci. 1998; 18:4155–4165. [PubMed: 9592095]

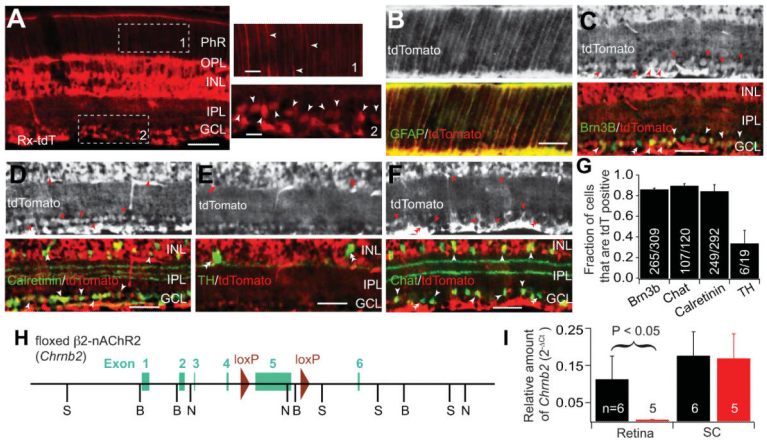

Figure 1. Reduced *Chrnb2* transcription in retina of Rx-β2cKO mice

(A-G) Expression of Cre in retina driven by Rx promoter. **(**A) Cre expression was examined by crossing Rx-Cre mice with a tdTomato reporter mouse. Cre was strongly expressed in the ganglion cell layer (GCL) and inner nuclear layer (INL). Fluorescence was also found in the inner plexiform layer (IPL) and outer plexiform layer (OPL). Representative areas in the photoreceptor layer (PhR) and the GCL, indicated by area 1 and 2, respectively, are enlarged and shown at right. Arrowheads indicate radial fibers extending into the PhR layer and somas in the GCL, respectively. (B) The radial extending filaments were likely Müller glia cells as they were co-localized with glial filbrillary acidic protein **(**GFAP). (C-F) Co-localization of tdTomato with Brn3B, Calretinin, Tyrosine Hydroxylase (TH) and Choline Acetyltransferase (Chat) in the INL and the GCL. Single arrowheads indicate immunostained neurons expressing tdTomato and double arrowheads indicate inmmunolabeled neurons that did not express tdTomato. (G) Fraction of Brn3B, Chat, Calretinin, and TH positive cells that also expressed tdTomato. (H) Design of floxed β2-nAChR (floxed *Chrnb2*) mice. Two loxP sites were incorporated into the targeted *Chrnb2* gene flanking approximately 2.2 kb DNA surrounding exon 5. (I) The relative amount of *Chrnb2* mRNA was significantly reduced in the retina of Rx-β2cKO mice compared to wild type controls. However, C*hrnb2 mRNA levels* were comparable in the SC of Rx-β2cKO and control mice. Scale = 50 μm.

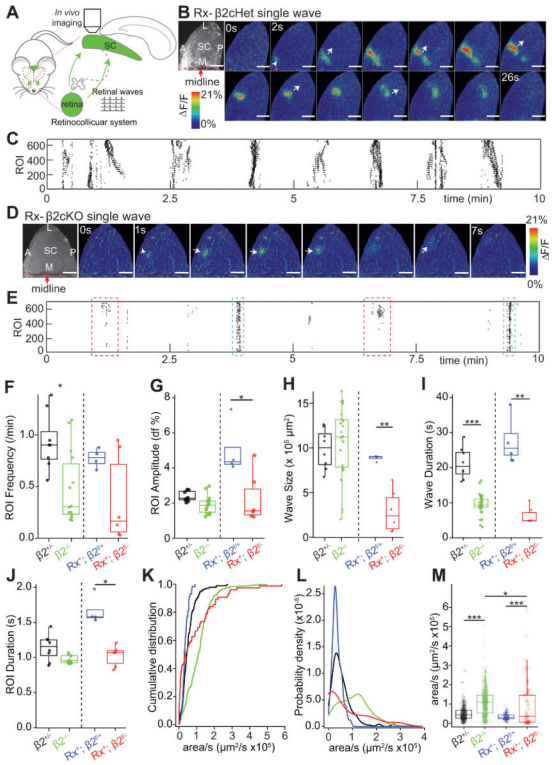

Figure 2. Truncated spontaneous retinal activity in Rx-β2cKO mice

(A) Retinal wave-imaging schematic. Retinal waves were imaged *in vivo* in topographically mapped axon arbors of RGCs in the upper layers of the SC through a craniotomy. Calcium activity in RGC axons in the SC were measured through viral expression of GCaMP6 in RGCs. (B) Example single-wave montages from a P5 conditional heterozygous (Rx-Cre^{+},β2$^{flox/+}$: Rx-β2cHet) mouse. Grayscale images on left (top) show craniotomy over the SC. White arrowhead shows onset and arrows indicate propagation of retinal wave front. A clear propagating wave front was typical in heterozygous mice. Movie frames shown in montage at 2s interval. All movies were acquired at 5 Hz. (C) Raster plot of 10 min recordings from the same mouse. Each row in the raster corresponds to one 10×10 μm region of interest (ROI) in the indicated hemisphere. (D) Example single-wave montage from a P5 conditional knockout (Rx-Cre^{+},β2$^{flox/-}$: Rx-β2cKO) mouse. Grayscale images on left (top) show craniotomies over SC. White arrowhead shows onset and arrows indicate propagation of retinal wave front. In this particular case, a small wave propagated over the SC with a noticeable wave front. Movies were acquired at 5 Hz and frames in montage are at 1s intervals. Scale bars, 200 μm. (E) Raster plot of 10 min recordings from the mouse shown in D. Each row in the raster corresponds to one 10×10 μm region of interest in the indicated hemisphere. Some small wave activity (as indicated by red dashed lines) in Rx-β2cKO mice show typical, slow, propagating dynamics, whereas the large waves (examples outlined by blue dashed lines) demonstrate fast, “flashy” dynamics. Spontaneous activity was less frequent (F) and of lower amplitude (G) in Rx-β2cKOs and β2KOs compared with their heterozygous controls. (H) Average wave size was much smaller in Rx-β2cKOs than their littermate heterozygous controls. P<0.01, student t-test, comparing between Rx-β2cKO and littermate heterozygous controls, and P >0.05 comparing between β2KOs and littermate

heterozygous controls. (I) Wave durations were shorter in Rx-β2cKOs and β2KOs than their littermate heterozygous controls, respectively. $P<0.05$, student t-test, comparing between Rx-β2cKO and its littermate heterozygous controls, and between β2KOs and their littermate heterozygous controls. (J) The duration of spontaneous activity measured in each ROI was shorter in Rx-β2cKOs but not β2KOs compared with their heterozygous controls. (K) and (L) Cumulative distribution and histograms of wave propagation speed (measured by coverage area per second), respectively. Spontaneous wave activity in heterozygous mice (both $\beta2^{+/-}$ and $\beta2^{flox/+}$, Rx-Cre^{+}) had homogeneous propagating dynamics, with a narrowly distributed peak between 0 and 1 $\mu m^2/s$. In contrast, the propagation speed in β2KO mice is significantly higher than in heterozygous controls, peaking between 1 and 2 $\mu m^2/s$. Most spontaneous waves in Rx-β2cKO mice propagate normally, with a peak between 0 and 1 $\mu m^2/s$, while some waves rapidly sweep through the SC, like in β2KO mice, generating a wide distribution with a peak similar to the β2 heterozygous controls and a long tail more typical of β2KO mice. (M) The average wave propagation speed in Rx-β2cKO mice was faster than that of Rx-β2cHET mice, but was slightly slower than in β2KO mice. Scale = 400 μm.

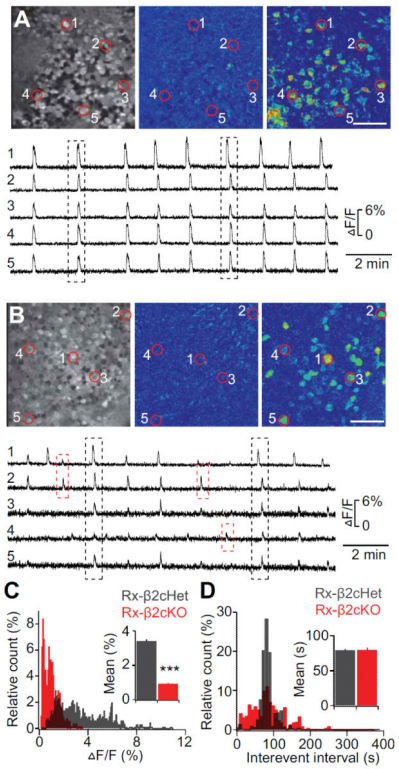

Figure 3. Weak and less regular Ca^{2+} activity *in vitro* in Rx-β2cKO mice

(A) and (B) Example spontaneous calcium activity imaged *in vitro* in retinas of a Rx-β2cHet (β2flox/+; Rx-Cre+) and a Rx-β2cKO mouse, respectively, at P5. Representative calcium images of spontaneous wave activity in top panels and calcium events of five example neurons (circled in red) plotted in bottom panels. Calcium events were highly correlated throughout the recording in heterozygous retinas. Although correlated calcium events (black dashed line boxes) were also found in Rx-β2cKOs, many events with relatively small amplitude (red dashed line boxes) occurred outside of correlated wave activity. (C) Histograms of the amplitudes of calcium events in Rx-β2cHets and Rx-β2cKOs at P5-6. Inset shows the mean amplitudes of calcium events in these two genotypes. The amplitude of calcium events was significantly smaller in Rx-β2cKOs than in heterozygous controls ($P<0.0001$, K-S test and Student t-test for cumulative distribution and mean, respectively). (D) Histograms of inter-event intervals of Rx-β2cHet and Rx-β2cKO mice. Inset, mean inter-event interval of calcium activities. Calcium events occurred irregularly in the Rx-β2cKOs relative to heterozygous controls as demonstrated by a broader distribution ($P<0.001$, K-S test). However, the mean inter-event interval was comparable between Rx-β2cKOs and heterozygous controls ($P>0.05$, Student t-test**)**. Scale = 50 μm.

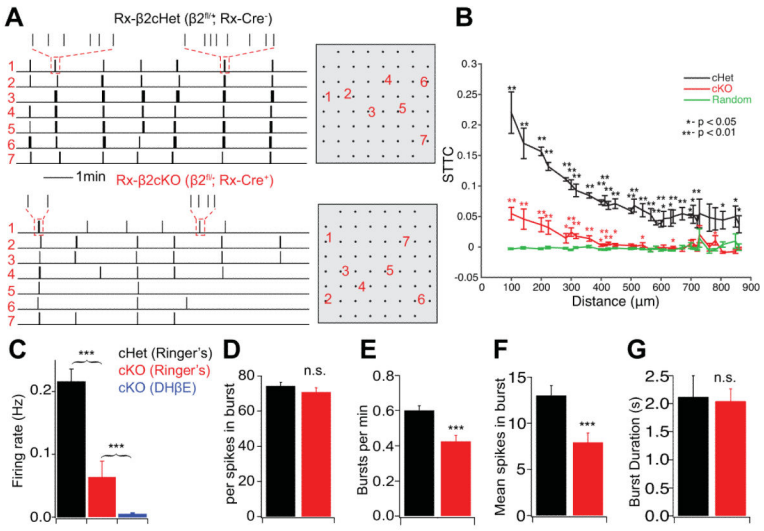

Figure 4. Reduced spiking activity in Rx-β2cKO retinas

RGC spiking activity was measured *in vitro* using a multielectrode array system. (A) Examples of bursting activity in seven RGCs recorded from a Rx-β2cHet control (top) and a Rx-β2cKO (bottom) mouse retina at P4. RGC activity was synchronized across the entire multielectrode array (shown in grey at right) in the Rx-β2cHet control, while many bursts were only locally correlated in the Rx-β2cKO. (B) Spike time tiling coefficient (STTC) for RGC activity in Rx-β2cKOs (red) and Rx-β2cHet (black) controls. The spontaneous activity in neighboring RGCs was significantly correlated in Rx-β2cKO mice (red * - compared to randomized), but was not correlated above chance at longer distances between RGCs. Rx-β2cHet spiking activity was significantly correlated at most distances and was more highly correlated than Rx-β2cKO activity (black *) even at shorter distances. (C) The overall firing rate in Rx-β2cKO (red) mice was reduced to less than 30% of that observed in Rx-β2cHet (black) controls. The remaining spiking activity was mediated by nAChRs, as it was completely blocked by DHβE, a nAChR specific antagonist. (D) There were a similar number of spikes occurring within bursts in Rx-β2cKO (red) and Rx-β2cHet (black) mice. However, the number of bursts (E) and the average spikes in a burst (F) was significantly reduced in Rx-β2cKO mice ($P<0.001$, Student t-test). (G) Burst duration was comparable between Rx-β2cKO and Rx-β2cHet mice. Inter-electrode distance = 100 μm.

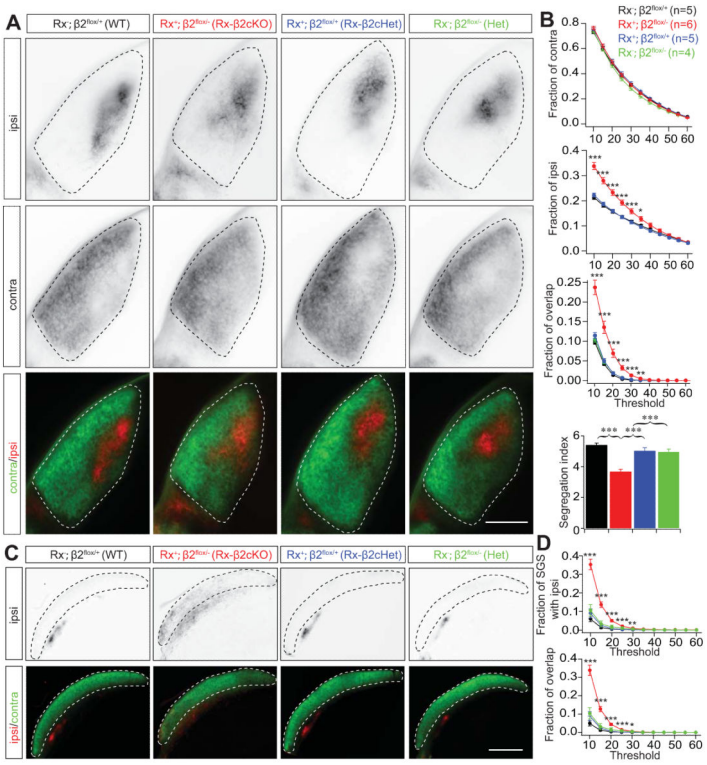

Figure 5. Disrupted eye-specific segregation in Rx-β2cKO mice

Eye-specific segregation was examined by anterograde labeling of RGC axonal projections to the dLGN and the SC by intraocular injection of CTB-488 and CTB-555 into the right and left eyes, respectively. (A) Representative fluorescence images of ipsilateral (top), contralateral (middle) and both contralateral (green) and ipsilateral RGC projections (red) together (bottom) in the dLGN of WT (Rx-Cre^{-};β2$^{flox/+}$), heterozygous (Rx-Cre^{+};β2$^{flox/+}$ or Rx-Cre^{-};β2$^{flox/-}$), and Rx-β2cKO (Rx-Cre^{+};β2$^{flox/-}$) mice at P8. (B) Summary quantification of the fraction of the ipsilateral, contralateral and overlap projections in the dLGN at P8. Axons of ipsilateral projections occupied a larger fraction of the dLGN and overlapped more with projections from the contralateral eye in Rx-β2cKO mice than in littermate WT and heterozygous controls. The segregation index for retinal projections to the dLGN in Rx-β2cKO mice was also significantly lower than that of WT and heterozygous controls at P8. (C) Representative projection patterns of RGCs from the two eyes in the SC of WT, heterozygous, and Rx-β2cKO mice. RGC axons from the contralateral eye arborize in the superficial layer of the SC (green in bottom) and axons from the ipsilateral eye project to the lower layer of the SC (top panel and red in bottom). There was very little overlap of projections from the two eyes in the SC in the WT and heterozygous controls. In Rx-β2cKO mice, the projections from the ipsilateral eye extended into the upper layer and overlapped with projections from the contralateral eye. (D). Summary quantification of ipsi projections in the SGS layer (top) and the fraction of overlaped projections (bottom) in the WT, heterozygous, and Rx-β2cKO mice. Scale = 500 μm.

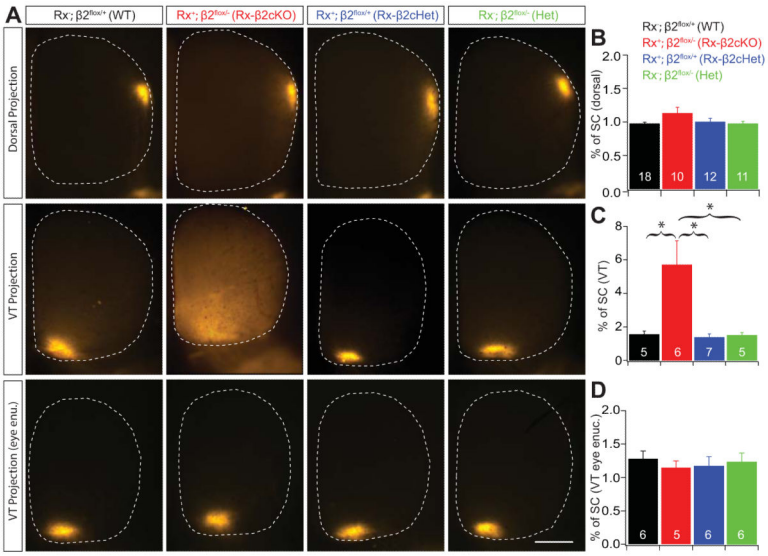

Figure 6. Normal retinotopic refinement in the SC of Rx-β2cKO mice

Retinotopy was investigated by focal injections of a small amount (2.3nl) of fluorescence dye (DiI) into indicated regions of the retina, and the size of RGC axon target zones in the SC were quantified in WT, Heterozygous (Rx-β2cHet and β2Het) and Rx-β2cKO mice. (A) Examples of target zones of a small group of RGCs in the dorsal (top), ventral-temporal retina (middle) in WT, Rx-β2cKO and heterozygous mice. There was no difference in the target zone size of dorsal projections in the four groups of mice (top), whereas the target zone of the ventral-temporal projection was significantly enlarged in Rx-β2cKO mice (middle). (B) and (C) Summary quantification of target zone sizes (% of SC) of dorsal and ventral-temporal projections, respectively. (A-bottom) and (D) Examples and summary quantification of ventral-temporal projections following monocular ipsilateral eye enucleation. The target zone of ventral-temporal RGC projections to the SC in Rx-β2cKO mice was not significantly different from WT and heterozygous controls after ipsilateral eye enucleation. Scale = 500 μm.

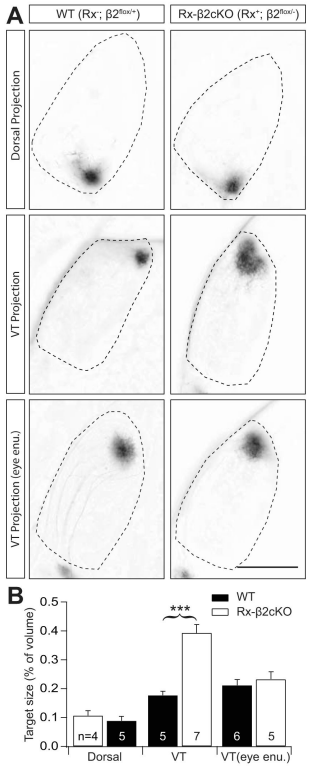

Figure 7. Normal retinotopic refinement in the dLGN of Rx-β2cKO mice

Retinotopy in the dLGN was investigated by focal injections of a small amount (2.3nl) of fluorescence dye (DiI) into indicated regions of the retina and the size of RGC axon target zones in the dLGN was quantified in WT (Rx-Cre^{-}; β2$^{flox/+}$) and Rx-β2cKO mice. (A) Examples of target zones of a small group of RGCs from the dorsal (top) and ventral-temporal (VT) retina (middle) in WT and Rx-β2cKO mice. There was no difference in the size of target zones for dorsal projections between these two groups of mice (top), whereas the target zone for the ventral-temporal projections was significantly enlarged in Rx-β2cKO mice (middle). Following ipsilateral eye enucleation (bottom), the ventral-temporal target zone in Rx-β2cKO was similar to WT mice. Scale = 500 μm. (B) Summary quantification of target zone sizes (% of dLGN volume) for dorsal projections and ventral-temporal (VT) projections with and without ipsilateral eye enucleation. VT projections in Rx-β2cKO mice were significantly enlarged compared to WT mice, but were no different following monocular enucleation.

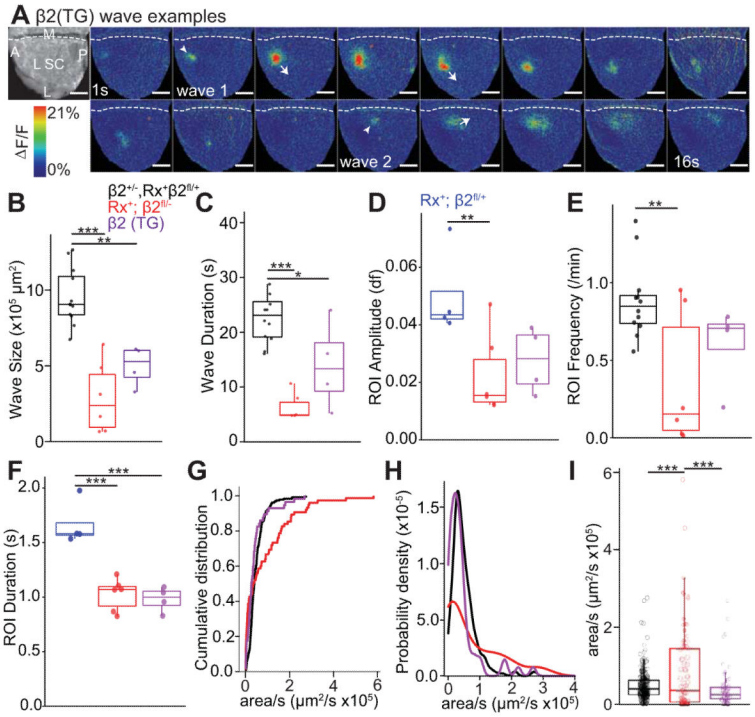

Figure 8. Truncated spontaneous waves in β2(TG) mice

Spontaneous RGC waves were recorded *in vivo* in the SC. GCaMP6 was expressed in RGCs through viral transfection. (A) Example wave montages from a P5 β2(TG) mouse. Grayscale image on left (top) shows the craniotomy over SC. White arrowheads show onsets and arrows indicate wave fronts of two local propagating waves. Movie frames shown in montage at 1s interval. Waves of β2(TG) mice were smaller (B, $P<0.01$ for comparison between β2(TG) and β2 heterozygous controls) and briefer (C, $P<0.05$ for comparison between β2(TG) and β2 heterozygous controls). The frequency (E) of calcium events in each ROI were comparable between β2(TG) and β2 heterozygous controls, while event duration (F) was lower ($P<0.001$) and calcium signal amplitude trends lower ($P=0.097$) in β2(TG) mice. (G) and (H) Cumulative distribution and histogram curves of wave propagation speed, measured as coverage area per second in β2 heterozygotes, β2(TG) and Rx-β2cKOs. The distribution of wave propagation speed in β2(TG) mice was similar to that in β2 heterozygotes (Rx-β2cHets), but was significantly different from Rx-β2cKO ($P<0.001$). (I) Average wave propagation speed was higher in Rx-β2cKO than in β2(TG) and in Rx-β2cHet ($P<0.01$, 0.001). Scale = 400 μm.

Table 1

Genotype	Wave Frequency	Wave Size	Wave Propagation Character	Correlation Index/Spike time tiling coefficient	Retinotopy	Eye-Specific Segregation
Wild-type or Het	~1/min in SC[6]	~1mm^2 in SC[6]	Slowly propagating[5]	Local correlations[7]	Fine	Little or no overlap after eye opening
β2 KO	Lower[6]	Larger[6]	Fast, flashing[6]	Lower at shorter distance, likely higher at longer distance[2,3,7], but see[1,4]	Disrupted, larger target zones[1], binocular competition independent[4]	Very disrupted, overlapped[1]
PiccTG	Normal[4]	Smaller[4]	Slowly propagating[4]	Lower at shorter and longer distance[4,7]	Normal, binocular competition dependent[4]	Disrupted, overlapped[4]
Rx-β2cKO	Lower	Smaller	Both slowly propagating and fast flashing	Lower at shorter and longer distance	Normal, binocular competition dependent	Disrupted, overlapped
Pax6α$^+$-β2cKO Cre positive KO region	Absent[6]	-	-	-	Disrupted[6]	Disrupted, overlapped[6]
Pax6α$^+$-β2cKO Cre negative Het region	Normal[6]	Smaller[6]	Slowly propagating[6]	-	Normal[6]	Disrupted, overlapped[6]

[1] – McLaughlin et al., 2003

[2] – Sun et al., 2008

[3] – Stafford et al., 2009

[4] – Xu et al., 2011

[5] – Ackman et al., 2012

[6] – Burbridge et al., 2014

[7] – Cutts et al., 2014